Dynamic Dimensionality Identification for Quantum Control

Jonathan Roslund* and Herschel Rabitz
Department of Chemistry, Princeton University, Princeton, New Jersey 08544, USA
(Received 11 April 2013; published 7 April 2014)

The control of quantum systems with shaped laser pulses presents a paradox since the relative ease with which solutions are discovered appears incompatible with the enormous variety of pulse shapes accessible with a standard pulse shaper. Quantum landscape theory indicates that the relevant search dimensionality is not dictated by the number of pulse shaper elements, but rather is related to the number of states participating in the controlled dynamics. The actual dimensionality is encoded within the sensitivity of the observed yield to all of the pulse shaper elements. To investigate this proposition, the Hessian matrix is measured for controlled transitions amongst states of atomic rubidium, and its eigendecomposition reveals a dimensionality consistent with that predicted by landscape theory. Additionally, this methodology furnishes a low-dimensional picture that captures the essence of the light-matter interaction and the ensuing system dynamics.

DOI: 10.1103/PhysRevLett.112.143001 PACS numbers: 33.80.-b

The control of quantum systems with optimally shaped laser pulses has proven remarkably effective at manipulating molecular dynamics in chemical, biological, and material environments [1]. High-finesse quantum control operates by managing the interference of multiple system states through their coupling to a shaped temporal field. The outcome of this light-matter interaction could independently draw upon each resolvable temporal or spectral field component, and the corresponding effort required to search for such a field ostensibly grows exponentially with the number of controllable elements. In practice, however, the discovery of an efficacious field typically necessitates only several thousand experimental evaluations irrespective of the particular system, which is a conspicuously small subset of the prodigious number of possible fields (e.g., [2–7]). Resolution of this paradox lies at the heart of understanding how an optimal field communicates with quantum systems and is paramount for extending control techniques to complex systems of general interest. Toward this end, quantum control landscape theory [8] predicts that the true search space dimensionality is not commensurate with the number of employed spectral elements, but is rather related to the number of system states directly participating in the controlled transition. The structure of this reduced-dimensional space may be gleaned by observing the sensitivity of the control yield to all of the parameters describing the pulse. If effective pulse shapes can be rapidly assembled from a small set of fundamental components, quantum control may find widespread adoption in a variety of applications, including high-finesse detection, material transformations, and chemical control. This Letter details the extraction of a low-dimensional control space for manipulating atomic excitation and, in doing so, substantiates the prediction of quantum landscape theory for a system of known dimension.

With an expanding repertoire of experimental control demonstrations, considerable effort has focused on discovering a natural set of reduced-dimensional control variables as a way to more thoroughly understand the controlled dynamics. One approach toward this goal is to examine the fitness landscape $J(\vec{x})$, which is the control yield as a function of the adjustable field parameters $\vec{x}$ [9,10]. The fitness landscape provides an intuitive picture as to how various components $\vec{x}$ of a shaped pulse synergetically interact with a quantum system to optimize a process [11–14]. A number of studies have turned to the high-dimensional topology of these landscapes as a means to reduce the search dimensionality. By examining the incremental refinements in pulse structure as a learning algorithm navigates the underlying landscape, dimensionality reduction has been achieved with several approaches that include utilizing multivariate statistics to monitor the evolution of the pulse [15,16], exerting selection pressure during the learning process [17–19], and applying *post facto* statistical analysis to the algorithm trajectory [20,21].

Each of these methodologies, however, convolves information retrieved about the fitness landscape with the dynamics of a particular optimization algorithm. Moreover, quantum landscape theory affirms that a rigorous connection between the search landscape and controlled dynamics is only possible in the immediate vicinity of the extrema. In particular, it is the landscape curvature that carries all of the information necessary to characterize the light-matter interaction and succeeding system dynamics [10]. In what follows, the landscape curvature is empirically measured and used to validate a fundamental theorem about the landscape itself.

The fitness landscape search dimensionality is tacitly taken as the number of independent control directions to which the target yield is sensitive. Such sensitivity

information is naturally revealed by the critical topology of the fitness landscape. Toward this end, the fitness landscape in the neighborhood of an extremum $\vec{x}_0$ is well approximated by the local Hessian $\mathcal{H}$, which is the matrix of landscape second derivatives: $J(\vec{x}_0+\vec{x}) \simeq J(x_0) + \frac{1}{2}\vec{x}^t\mathcal{H}|_{\vec{x}_0}\vec{x}$ [9]. A measurement of this matrix thus provides a well-defined entry point for understanding the intricacies of an arbitrarily high-dimensional fitness search landscape and establishing whether its true dimensionality equals the number of employed pulse shaper elements or rather is a lower value as assessed by landscape theory. It is important to stress that the Hessian is not obtained with a perturbation expansion about a null field, but rather a differential modification about the optimal field $\vec{x}_0$. Thus, following the application of $\vec{x}$, the system continues to evolve in the same dynamical regime as with the optimal field, which may include strong field effects.

Quality, noise-robust second-order derivatives are obtained with statistical moments built up from a local sampling of the fitness landscape [22]. Consider a random sampling about an extremum $\vec{x}_0$ where the variates $\vec{x}$ are drawn from statistically independent, symmetric probability distributions, i.e., $P(\vec{x}) = p(x_1)p(x_2)\ldots p(x_D)$ and $p(x_i) = p(-x_i)$. In the case of Gaussian sampling, i.e., $p(x_i) = \mathcal{N}(0,\sigma^2)$, the Hessian is well approximated by a yield-weighted correlation matrix:

$$\mathcal{H}_{ij} = \left.\frac{\partial^2 J}{\partial x_i \partial x_j}\right|_{\vec{x}_0} \simeq \frac{\langle x_i x_j [J(\vec{x}_0+\vec{x}) - \langle J\rangle]\rangle}{\sigma^4} + \sigma^2 \epsilon_{ij}, \quad (1)$$

where the error ϵ_{ij} implicit to this method consists of fourth-order derivative terms (see the Supplemental Material [23]). Given a narrow sampling distribution (i.e., $\sigma \to 0$), the correlation matrix approaches the true Hessian $\mathcal{H}$.

When considering transitions amongst pure system states, quantum landscape theory predicts a Hessian rank (i.e., number of meaningful uncoupled search directions) of at most $2N-2$ at a fitness maximum, where N is the number of resolvable system states directly participating in the controlled transition. Conversely, the Hessian rank at a fitness minimum is expected to be independent of N and has a value no larger than 2 [9,10]. At either landscape extremum, the Hessian eigenvectors associated with the nonzero eigenvalues encapsulate the most salient features of the spectral variables. Considering that pulse shapes are typically constructed with upwards of ~100 independent spectral amplitude or phase values, the Hessian matrix for a prototypical control process, which might involve transitions amongst several electronic or vibrational states ($N \lesssim 10$), is expected to be exceedingly sparse and exhibit a large null space.

In order to validate this prediction, the Hessian is directly measured at both the fitness minima and maxima for two-photon electronic transitions of atomic rubidium. Rubidium possesses two independently accessible pathways from the ground $5S$ state to the target $5D$ state [24], and spectral phase shaping is utilized to both maximize and minimize the transition probability to the $5D$ state [25]. The retrieved curvature at these extrema is directly relatable to the known atomic structure. Importantly, the strategy for the measurement of the landscape curvature is general, and an atomic system consisting of a small number of states is considered solely to enable a well-defined comparison to theory.

Laser pulses from a Ti:sapphire oscillator centered at 780 nm and with a bandwidth $\Delta\lambda = 47$ nm (FWHM) are phase modulated with 80 independent pixels (~1.2 nm/pixel resolution) using a liquid-crystal pulse shaper. These linearly polarized pulses are focused to a spot diameter of 20 μm in a 25 mm quartz Rb vapor cell maintained at 90 °C. The pulses induce $5S \to 5P \to 5D$ electronic transitions, and the bandwidth provides sufficient spectral coverage to activate both resonant pathways [Fig. 1(a)] to the $5D$ state. Population transferred into the $5D$ states rapidly undergoes relaxation to $6P$ states.

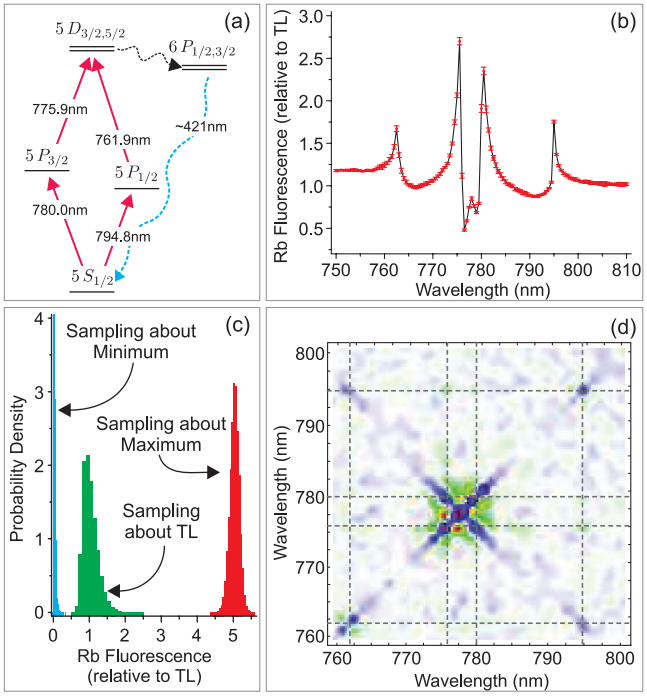

FIG. 1 (color). Broadband femtosecond excitation of rubidium may exploit two distinct spectral pathways to populate the $5D$ states (a). A scan of a π-phase step across the bandwidth (b) identifies the four resolvable system states depicted in (a). Sampling in the immediate vicinity of an optimum (c) is used to construct a correlation matrix that approximates the underlying Hessian. The reconstructed Hessian matrix at the landscape maximum (d) reveals couplings corresponding to the two excitation pathways illustrated in (a). The gray lines correspond to the transition frequencies depicted in (a).

The 80 MHz pulse train from the oscillator is modulated at 1 kHz with an optical chopper and the resultant $6P \rightarrow 5S$ fluorescence is imaged onto a photomultiplier tube in a direction orthogonal to the incident beam and lock-in detected.

Second-order perturbation theory shows that the probability amplitude $a_d(t)$ of the $5D$ electronic state at a time much longer than the duration of the pulse is $a_d(+\infty) \propto \int_{-\infty}^{\infty} d\omega(E(\Omega)E(\Omega_{ds}-\Omega)/\omega_{ps}-\omega)$, where $E(\Omega)$ is the complex spectral amplitude of the shaped pulse, $\Omega = \omega - \omega_0$, and $\Omega_{ds} = \omega_{ds} - 2\omega_0$ [26]. This transition amplitude experiences a π-phase shift between frequencies above and below a resonant intermediate frequency ω_{ps}. For an unshaped pulse, a destructive quantum interference results for photon pairs where one member is higher in frequency and the other lower than this intermediate transition frequency. However, if a π-phase shift is imprinted onto the field $E(\Omega)$ at either ω_{ps} or $\omega_{ds} - \omega_{ps}$, the phase shift acquired by the system is negated and constructive interference is achieved in the $5D$ state. Accordingly, an increase in the fluorescence signal while a π-phase step is scanned across the spectral bandwidth is indicative of an intermediate transition, and such a scan [Fig. 1(b)] reveals that the present configuration resolves four discrete system states ($N = 4$) with population simultaneously traveling through both resonant pathways to the target $5D$ state.

Following each optimization, a random sampling of the landscape in the immediate vicinity of the optimum is conducted with 80 individual spectral phase variables. Although the variates are drawn from distributions with identical sampling widths (i.e., $\sigma = 0.025 \cdot 2\pi$), the yield deviations at the landscape maximum, minimum, and about the transform-limited (TL) pulse exhibit considerable differences in robustness [Fig. 1(c)]. Following $\sim 3 \times 10^4$ random samplings, the Hessian matrix at the landscape maximum is reconstructed according to Eq. (1) [Fig. 1(d)] and exhibits structure at each of the four resonant wavelengths (diagonal elements) as well as the intermediate couplings. These peaks indicate that the $5D$ state is populated through known level couplings [27].

Since the yield-weighted correlation is a statistical moment-based technique, the individual elements of the reconstructed Hessian are expected to exhibit $1/\sqrt{M}$ convergence, where M is the number of locally sampled points on the fitness landscape. As such, the Hessian spectrum may be examined as the sample size M is increased as seen in Fig. 2(a) for the Hessian matrix about the landscape maximum. Two classes of eigenvalues are discernible. The first group, which contains the preponderance of the collection, converges toward a mean value of zero. The second group consists of six eigenvalues that converge toward nonzero values. In the limit of infinite sampling, the extrapolated spectra at the landscape maximum and minimum are shown in Fig. 2(b) (see the Supplemental Material [23]). The Hessian is exceedingly

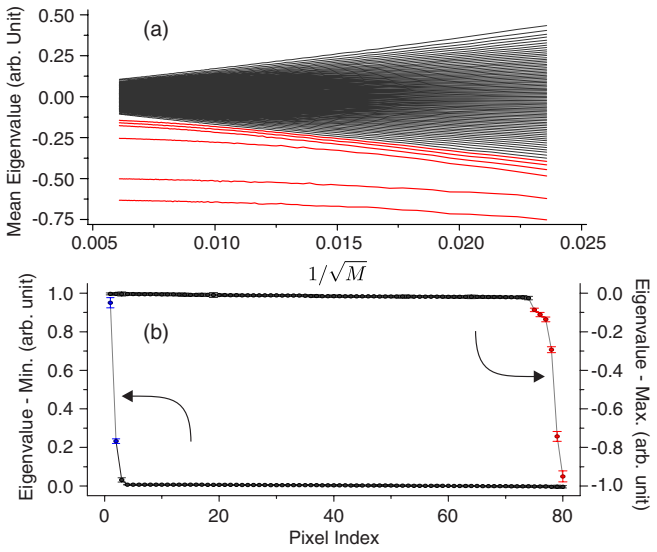

FIG. 2 (color online). (a) Convergence behavior for mean Hessian eigenvalues at the landscape maximum as the sample size M increases. Six eigenvalues (red) are distinguishable from the bulk (black) that converge toward a value of zero. (b) The extrapolated Hessian spectra at the landscape maximum (red) and minimum (blue) possess six and two nonzero eigenvalues, respectively, which is consistent with the predictions of landscape theory.

sparse at the two extrema, and in both cases, the retrieved rank agrees with that predicted by quantum landscape theory for a Hilbert state dimension of $N = 4$ [9,10]. Hessian eigenvectors corresponding to these extrapolated eigenvalues are depicted in Fig. 3.

The three most yield-sensitive control directions at the landscape maximum (i.e., vectors 78—80 of Fig. 3) are dominated by the $5S \rightarrow 5P_{3/2} \rightarrow 5D$ transition pathway (components *i* and *ii*). This is due to the larger transition dipole moments associated with this pathway and the fact that the spectral amplitude is centered around this route. The subsequent three directions at the maximum (i.e., vectors 75—77) are largely associated with the alternative $5S \rightarrow 5P_{1/2} \rightarrow 5D$ pathway (components *iii* and *iv*). These two pathways are not independent, however, and the simultaneous presence of both transitions is evident in eigenvectors 76 and 77. Conversely, the most efficient ascent from the landscape minimum makes independent use of both resonant pathways (Fig. 3). Rapid yield increase is associated with the $5S \rightarrow 5P_{3/2} \rightarrow 5D$ pathway (components *i* and *ii*), which is consistent with it also being the most sensitive direction at the maximum.

These eigenvectors also furnish a well-defined, reduced dimensional basis. The yield variations corresponding to landscape trajectories taken in the direction of these eigenvectors are shown in Fig. 4. At the landscape maximum, the observed yield variations of the leading six eigenvectors [Fig. 4(a)] agrees with the extrapolated eigenvalue ordering presented in Fig. 2(b). Small

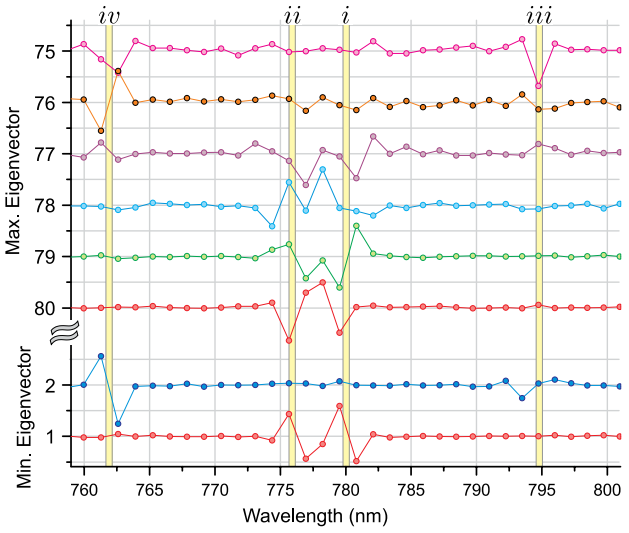

FIG. 3 (color online). Hessian eigenvectors corresponding to nonzero eigenvalues at the landscape maximum (top) and minimum (bottom). These eigenvectors reveal the most yield-sensitive control directions at their respective locations, and each eigenvector coordinates movement of all pulse shaper pixels. The four known resonant wavelengths of atomic rubidium are indicated as colored bars.

displacements of $\|\Delta\vec{\phi}_i\|$ reveal symmetric yield variations. These eigenvectors also provide a near one-dimensional pathway between the global minimum and maximum, which is likely explained by the similarity of the principal eigenvectors at the landscape extrema as seen in Fig. 3. For comparison, the Hessian matrix is also measured in the immediate vicinity of the TL pulse (i.e., $\vec{\phi}_0 = 0$), and trajectories along its two largest and smallest eigenvectors are shown in Fig. 4(b). Since the gradient is not zero at this location, the yield variations are no longer symmetric. Likewise, movement originating at the landscape minimum is illustrated in Fig. 4(c). These trajectories are also in agreement with the Hessian eigenvalue spectrum and confirm that the $5S \rightarrow 5P_{3/2} \rightarrow 5D$ resonant pathway provides the most rapid ascent to the target $5D$ eigenstate. An eigenvector selected from the control null space [black points in Figs. 4(a) and 4(c)] validates the relative yield insensitivity for movement in this direction.

The Hessian furnishes an effective model of disturbances that originate at the landscape maximum. As such, the role of a specific wavelength in the control process may be investigated by removing its contribution from the Hessian matrix. If the deactivation of a given wavelength changes the number of states participating in the transition, landscape theory dictates that the Hessian rank must adjust accordingly. For different configurations of deleted wavelengths, the observed rank contracts to a value in accordance with that predicted from landscape theory (see the Supplemental Material [23]).

Away from the critical structure, sensitivity information is embedded in the landscape gradient rather than the Hessian, and the number of nonzero Hessian eigenvalues is not rigorously relatable to the quantum system. As a result, a basis constructed from the Hessian at landscape positions other than at the extrema has no connection with the system dimensionality N. In this situation, the search dimensionality is dictated by the number of functions necessary to reconstruct the gradient in a chosen basis. In practice, an *a priori* basis selection reflective of the landscape structure is generally not evident. However, theoretical analysis shows that the gradient may also be expressed with $2N-2$ specific basis functions at all positions on the fitness landscape [28]. Consequently, the search dimensionality at any particular point on the landscape will be the same as that discovered at the extrema. This is consistent with the quasiglobal extent of the extrema eigenvectors as seen in Fig. 4, and renders them an effective basis elsewhere on the landscape.

It is important to stress that the Hessian rank prediction does not depend upon the strength of the light-matter coupling, and situations may arise in which the retrieved

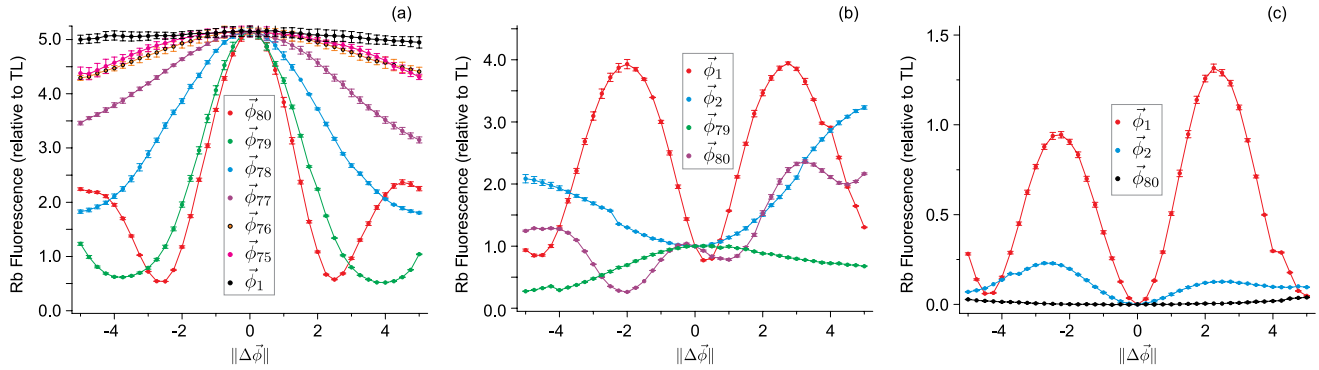

FIG. 4 (color online). Trajectories through spectral phase space at the landscape maximum (a), about the TL pulse (b), and at the landscape minimum (c). Trajectories assume the form $\vec{\phi}_i^{\,\mathrm{traj}}(\gamma) = \vec{\phi}_0 + \gamma\vec{\phi}_i$, where $\vec{\phi}_0$ is either an optimal phase [panels (a) and (c)] or zero phase [panel (b)], and $\vec{\phi}_i$ is the ith phase eigenvector of the Hessian. The Euclidean distance through phase space is $\|\Delta\vec{\phi}_i\| = \|\vec{\phi}_i^{\,\mathrm{traj}}(\gamma) - \vec{\phi}_0\| = \gamma$. In panels (a) and (c), the colors correspond to the eigenvectors of Fig. 3.

search dimensionality is not smaller than the original search space. Strong-field processes, including multiphoton transitions, are facilitated by the collection of all nonresonant states that are dipole coupled to the states of interest. Accordingly, the number of states N contributing to the nonresonant transition is exceedingly large, and the Hessian rank is predisposed to equal the number of available pulse shaper elements [29]. Conversely, a few level system nonresonantly coupled to other states should display a continuous Hessian spectrum along with several discrete lines. In either situation, the spectral form of the Hessian should reveal the nature of the connections linking the initial and final states, and therefore provides important input for modeling the control process.

In conclusion, whereas quantum control optimizations outwardly appear to proceed in exceedingly high dimensions, the actual dimensionality is related to the number of involved system states, a number which has the potential to be quite small. Consequently, evolutionary algorithms are able to efficiently and rapidly navigate these spaces to discover capable pulse shapes. Knowledge of the true effective dynamic dimensionality should enable construction of simplified models describing the light-matter interaction, and such models will prove especially valuable for understanding the dynamics of complex control processes. The present observation of a dimensionality consistent with that predicted by quantum landscape theory provides the first experimental corroboration of the emerging theory and reinforces its positive projections for the capabilities of quantum control.

The authors acknowledge support from the ONR, NSF, and ARO.

*jroslund@princeton.edu

[1] P. Nuernberger, G. Vogt, T. Brixner, and G. Gerber, Phys. Chem. Chem. Phys. **9**, 2470 (2007).
[2] C. J. Bardeen, V. V. Yakovlev, K. R. Wilson, S. D. Carpenter, P. M. Weber, and W. S. Warren, Chem. Phys. Lett. **280**, 151 (1997).
[3] A. Assion, T. Baumert, M. Bergt, T. Brixner, B. Kiefer, V. Seyfried, M. Strehle, and G. Gerber, Science **282**, 919 (1998).
[4] R. Bartels, S. Backus, E. Zeek, L. Misoguti, G. Vdovin, I. Christov, M. Murnane, and H. Kapteyn, Nature (London) **406**, 164 (2000).
[5] T. Laarmann, I. Shchatsinin, A. Stalmashonak, M. Boyle, N. Zhavoronkov, J. Handt, R. Schmidt, C. P. Schulz, and I. V. Hertel, Phys. Rev. Lett. **98**, 058302 (2007).
[6] J. L. Herek, W. Wohlleben, R. J. Cogdell, D. Zeidler, and M. Motzkus, Nature (London) **417**, 533 (2002).
[7] V. I. Prokhorenko, A. M. Nagy, S. A. Waschuk, L. S. Brown, R. R. Birge, and R. D. Miller, Science **313**, 1257 (2006).
[8] H. Rabitz, M. Hsieh, and C. Rosenthal, Science **303**, 1998 (2004).
[9] T.-S. Ho and H. Rabitz, J. Photochem. Photobiol., A **180**, 226 (2006).
[10] H. Rabitz, T. S. Ho, M. Hsieh, R. Kosut, and M. Demiralp, Phys. Rev. A **74**, 012721 (2006).
[11] M. Wollenhaupt, A. Präkelt, C. Sarpe-Tudoran, D. Liese, and T. Baumert, J. Mod. Opt. **52**, 2187 (2005).
[12] T. Bayer, M. Wollenhaupt, and T. Baumert, J. Phys. B **41**, 074007 (2008).
[13] P. Marquetand, P. Nuernberger, G. Vogt, T. Brixner, and V. Engel, Europhys. Lett. **80**, 53001 (2007).
[14] D. Cardoza, C. Trallero-Herrero, F. Langhojer, H. Rabitz, and T. Weinacht, J. Chem. Phys. **122**, 124306 (2005).
[15] J. L. White, B. J. Pearson, and P. H. Bucksbaum, J. Phys. B **37**, L399 (2004).
[16] M. A. Montgomery, R. R. Meglen, and N. H. Damrauer, J. Phys. Chem. A **110**, 6391 (2006).
[17] D. Cardoza, F. Langhojer, C. Trallero-Herrero, O. L. A. Monti, and T. Weinacht, Phys. Rev. A **70**, 053406 (2004).
[18] F. Langhojer, D. Cardoza, M. Baertschy, and T. Weinacht, J. Chem. Phys. **122**, 014102 (2005).
[19] A. Lindinger, S. M. Weber, C. Lupulescu, F. Vetter, M. Plewicki, A. Merli, L. Wöste, A. F. Bartelt, and H. Rabitz, Phys. Rev. A **71**, 013419 (2005).
[20] R. A. Bartels, M. M. Murnane, H. C. Kapteyn, I. Christov, and H. Rabitz, Phys. Rev. A **70**, 043404 (2004).
[21] S. Weber, A. Lindinger, M. Plewicki, C. Lupulescu, F. Vetter, and L. Wöste, Chem. Phys. **306**, 287 (2004).
[22] J. Roslund and H. Rabitz, Phys. Rev. A **79**, 053417 (2009).
[23] See Supplemental Material at http://link.aps.org/supplemental/10.1103/PhysRevLett.112.143001 for the derivation of Eq. 1 as well as additional details regarding the convergence of the measured Hessian matrices.
[24] S. Clow and T. Weinacht, Phys. Rev. A **82**, 023411 (2010).
[25] R. S. Judson and H. Rabitz, Phys. Rev. Lett. **68**, 1500 (1992).
[26] N. Dudovich, B. Dayan, S. M. Gallagher Faeder, and Y. Silberberg, Phys. Rev. Lett. **86**, 47 (2001).
[27] P. Tian, D. Keusters, Y. Suzaki, and W. S. Warren, Science **300**, 1553 (2003).
[28] M. Hsieh, T.-S. Ho, and H. Rabitz, Chem. Phys. **352**, 77 (2008).
[29] O. M. Shir, J. Roslund, D. Whitley, and H. Rabitz, arXiv:1112.4454.